Journal of Materials Chemistry B

PAPER

View Article Online
View Journal | View Issue

Cite this: J. Mater. Chem. B, 2019, 7, 768

Au nanoparticle *in situ* decorated RGO nanocomposites for highly sensitive electrochemical genosensors†

Chiara Ingrosso,*[a] Michela Corricelli,[a] Francesca Bettazzi,[b] Evgenia Konstantinidou,[b] Giuseppe V. Bianco,[c] Nicoletta Depalo,[a] Marinella Striccoli,[a] Angela Agostiano,[ad] M. Lucia Curri[a] and Ilaria Palchetti[b]

Received 25th September 2018,
Accepted 2nd January 2019

DOI: 10.1039/c8tb02514b

rsc.li/materials-b

A novel hybrid nanocomposite formed by RGO flakes, surface functionalized by 1-pyrene carboxylic acid (PCA), densely and uniformly *in situ* decorated by Au NPs, that are concomitantly coordinated by the PCA carboxylic group, and by an aromatic thiol used as the reducing agent in the synthesis, both ensuring, at the same time, a stable non-covalent NPs anchorage to the RGO flakes, and an efficient interparticle electron coupling along the NP network onto the RGO, is reported. The obtained solution processable hybrid material is used to modify Screen-Printed Carbon Electrodes (SPCEs). The hybrid modified SPCEs, functionalized with a thiolated DNA capture probe, are tested in a streptavidin–alkaline-phosphatase catalyzed assay, for the detection of the biotinylated miRNA-221, and for its determination in spiked human blood serum samples. The proposed genosensor demonstrates a high sensitivity (LOD of 0.7 pM), attesting for a performance comparable with the most effective reported sensors. The enhanced sensitivity is explained in terms of the very fast heterogeneous electron transfer kinetics, the concomitant decrease of the electron transfer resistance at the electrode/electrolyte interface, the high electroactivity and the high surface area of the nanostructured hybrid modified SPCEs that provide a convenient platform for nucleic acid biosensing.

Introduction

Circulating nucleic acids are emerging as novel reliable biomarkers for early detection of many diseases, including cancer. Developing point-of-care, precise and rapid methods for their early diagnosis is an increasingly urgent requirement.[1] Among the different analytical methods proposed for point-of-care diagnostics, electrochemical biosensors are particularly interesting because of their simplicity, fast response, low detection limit (LOD), low cost and portability of the instrumentation.[2]

Nowadays, a vast literature attests for the application of graphene based electrodes in electrochemical sensing, due to their electrochemical stability, superior conductivity, high electrocatalytic activity, large potential window and remarkably fast heterogeneous electron transfer kinetics for various analytes, along with a good biocompatibility and environmental stability.[3] Due to the high chemical reactivity endowed by the aromatic platform, graphene is considered a robust scaffold for manufacturing original and highly functional hybrid materials with nanoparticles (NPs) and biomolecules.

Au NPs have been widely demonstrated ideal candidates for electrochemical (bio)sensing, due to their capability of binding biomolecules by means of chemical moieties (*i.e.* –SH, –NH_2, –COOH), the high rate of electron transfer kinetics at the electrode/electrolyte interface, and the excellent surface redox electrocatalytic activity, all amenable properties for the specific detection of (bio)molecules.[4] The decoration of graphene with metal NPs provides a very large electrochemically active surface area, and effectively accelerates electron transfers between electrodes and detection molecules, leading to a rapid and sensitive current response.[5] Au NPs decorated graphene sheets have been proved effective for detecting nucleic acids by hybridization events upon immobilization of thiol-modified biomolecules, such as thiol-tethered DNA capture probes.[4,6] Electrodes, modified with a hybrid material based on Au NPs,

[a] CNR-IPCF S. S. Bari, c/o Dep. of Chemistry, Università di Bari, via Orabona 4, I-70126 Bari, Italy. E-mail: c.ingrosso@ba.ipcf.cnr.it
[b] Dep. of Chemistry Ugo Schiff, Università degli Studi di Firenze, via della Lastruccia 3-13, 50019 Sesto Fiorentino, Firenze, Italy
[c] CNR-NANOTEC, c/o Dep. of Chemistry, Università di Bari, via Orabona 4, I-70126, Bari, Italy
[d] Dep. of Chemistry, Università di Bari, via Orabona 4, I-70126 Bari, Italy

† Electronic supplementary information (ESI) available: Electroactive area and electron transfer rate constant values of SPCEs, as bare and modified by PCA–RGO/Au NPs. CVs of TMB and H_2O_2 and amperometric detection of H_2O_2. Calibration curve of miRNA-221 in spiked human blood serum samples. See DOI: 10.1039/c8tb02514b

immobilized onto toluidine blue-surface decorated graphene oxide, have been demonstrated able to perform the electrochemical detection of multidrug resistance 1 gene by Differential Pulse Voltammetry (DPV), with a LOD of 2.95 pM.[6] GO flakes, surface decorated with Au NPs, grown *in situ* by a hydrothermal route, have been applied for the visible and label-free colorimetric detection of RNA sequences, with a LOD of 3.2 nM.[7]

In this work, a novel hybrid nanocomposite formed of Reduced Graphene Oxide (RGO) flakes, surface decorated with 3,4-dimethylbenzenethiol (DMBT)-capped Au NPs, has been prepared in order to combine the superior properties of the two components in an original composite, and it has been tested as genosensing platform.[8] RGO is a graphene derivative, that, although presenting structural defects, shows many of the relevant properties of graphene, concomitantly permitting its solution processing, both for fundamental studies and for technological applications.[9]

The hybrid nanostructures have been synthesized by means of a flexible *in situ* Au precursor reduction, which has been carried out in presence of the aromatic ligand DMBT, and of $NaBH_4$, and by using 1-pyrenecarboxylic acid as linker with the RGO platform.[10] The RGO flakes have been surface functionalized with PCA by means of a non-covalent approach, which relays on binding PCA on RGO by means of π–π interactions, for preserving the Csp^2 structure in RGO, and hence its peculiar properties.[11] PCA behaves as coupling agent between RGO and the growing NPs, as it is able to anchor to RGO, while its carboxylic group is available as heteronucleation and coordination site for the *in situ* synthesis of the Au NPs, concomitantly enabling the charge transfer between the hybrid components.[8,10] Finally, the thiol controls the geometry of the Au NPs, favors their anchorage onto the flakes thanks to π–π interactions, and, grants Au interparticle coupling, resulting in a conductive network onto the flakes.[12]

In this work, the colloidal PCA–RGO/Au NPs hybrid nanostructures have been prepared and characterized and, thanks to their solution processability, have been used to modify cost-effectively obtained Screen-Printed Carbon Electrodes (SPCEs). Remarkably, the PCA–RGO/Au NPs hybrid modified SPCEs can be used as disposable, in order to avoid fouling of the electroactive surface, and thus, the need of electrode regeneration. This fact is particularly important when clinical samples have to be analyzed, in order to avoid the undesired effect of serum proteins that can be non-specifically adsorbed on the electrode surface, undermining the sensitivity of an analytical assay.

The modified SPCEs have been thoroughly investigated, and have shown, compared to the PCA–RGO modified SPCEs, faster heterogeneous electron transfer (ET) kinetics at the interphase with the electrolyte, an increase in the conductivity, and an overall enhancement of the electrocatalytic properties.

The PCA–RGO/Au NPs modified SPCEs have been tested as sensitive genosensors of miRNA-221, a non-coding short RNA fragment that has been proposed as circulating biomarker for many types of cancer.

Many examples report the use of an enzyme signal-amplification route of the hybridization reaction for the determination of nucleic acid tumor markers.[13] The use of enzymes as labels has been recognized as very successful in bioassays, due to their ability to convert a single binding event, into multiple detectable molecules, thus turning into an amplified detection sensitivity and a low LOD.

For instance, determination of miRNA-21 involving a sandwich hybridization assay onto streptavidin magnetic beads, hybridization chain reaction amplification and amperometric detection, using peroxidase as enzymatic label on disposable SPCEs, has been reported with a dynamic linear range from 0.2 to 5.0 nM and a 60 pM LOD.[13b]

Graphene flakes deposited onto glassy carbon electrodes, coated by electro-deposited Au NPs, and then, subsequently, by an electro-polymerized PANI layer, have been found to capture 5′-SH and 3′-biotin labeled DNA probes, for electrochemically detecting BCR/ABL fusion gene in chronic myelogenous leukemia, by means of a streptavidin–alkaline phosphatase amplified assay. Oxidation currents of 1-naphthol, generated upon the hydrolysis of 1-naphthyl phosphate, have been monitored by DPV with a LOD as low as 2.11 pM.[4b]

For this purpose, a thiol-tethered DNA-capture probe has been immobilized onto the PCA–RGO/Au NPs modified SPCEs, and DPV investigation has evaluated the extent of the hybridization reaction with a biotinylated target miRNA-221 sequence in spiked human blood serum samples, through the detection of 1-naphthol, that is generated by streptavidin–alkaline phosphatase in presence of the 1-naphthyl phosphate enzymatic substrate.

Here, the manufactured hybrid nanomaterial modified SPCEs have demonstrated an advantageous electrocatalytic activity for the detection of the species that are typically involved in enzyme-amplified bioassays, specifically 1-naphthol, tetramethyl benzidine and H_2O_2.

Overall, the analytical performances, the diagnostic feasibility and reliability of the hybrid nanocomposite modified SPCEs have been assessed by means of enzyme signal-amplification for the determination of miRNA-221 in spiked serum samples, resulting in a remarkably low LOD, comparable with the lowest LODs reported for state of art sensors.[13c]

Results and discussion

Synthesis and characterization of the PCA–RGO/Au NPs hybrid nanocomposite

The Au NPs surface modified PCA–RGO flakes have been prepared by means of the *in situ* reduction of the $HAuCl_4 \times 3H_2O$ precursor, in presence of the aromatic 3,4-dimethylbenzenethiol (DMBT) capping ligand. In the synthesis, the Au(III) precursor is reduced to Au(I) by DMBT, and then to Au(0) by $NaBH_4$.[14] The Au NPs heteronucleate and grow at the oxygen containing functionalities of the PCA–RGO sheets,[15] and the aromatic DMBT ligand controls the NP morphology and size distribution during the synthesis, by coordination to the NP surface,[14] and concomitantly, it provides further anchorage of the NPs to the RGO sheets, by means of π–π interactions, granting interparticle electronic coupling along the NPs network (Scheme 1).[12]

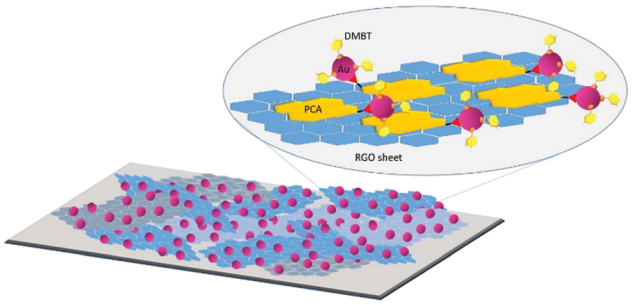

Scheme 1 Sketch of the PCA–RGO/Au NPs hybrid nanostructures and of the electrodes, based on porous multilayer stacks of PCA–RGO sheets, decorated with the DMBT-coated Au NPs.

Fig. 1(A) shows the Transmission Electron Microscopy (TEM) micrograph of the achieved PCA–RGO/Au NPs hybrid nanocomposite, as mainly formed of micro-meter large sheet like structures, coated by higher contrast round shaped nano-objects, 2.8 ± 0.6 nm in mean diameter. Such a morphology is reasonably accounted for by PCA–RGO flakes, homogeneously and densely coated by Au NPs, growing onto the flakes with a uniform morphology and a narrow size distribution, as assessed by the statistical analysis reported in the inset of Fig. 1(A).

The TEM micrograph (Fig. 1(A)) shows also higher contrast fine lines across the surface of the flakes, that can be reasonably ascribed to folded edges and wrinkles originated from mechanical lattice deformations likely caused by structural defects,[16] or by crumpling up of the flakes, upon deposition onto the TEM grid, after solvent drying. Finally, high contrast areas can be observed, which may be likely due to the overlap of few sheets of graphene, and to the self-assembly of the NPs in porous multilayer stacks, forming by π–π interactions among the DMBT ligand molecules coordinating the NP surface, and with Au NPs serving as nano-spacers between the PCA–RGO sheets.

The stability of the interactions responsible of the Au NPs immobilization onto the PCA–RGO flakes is demonstrated by the capability of the hybrid nanostructures to sustain the precipitation procedure, described in the Experimental section, implemented to separate, by centrifugation, the free Au NPs, homonucleated in the reaction mixture, from the Au NPs heteronucleated on the PCA–RGO flakes.

A control experiment has been performed to assess the involvement of the oxygen containing functionalities of the PCA–RGO flakes on the formation, and then, anchorage of the Au NPs onto the sheets. In particular, the *in situ* synthesis of the Au NPs has been performed onto bare RGO flakes. Fig. S1(A) of the ESI† reports the TEM image of the achieved RGO flakes after the *in situ* synthesis, assessing almost the lack of Au NPs anchored onto the surface of the bare sheets. This result demonstrates the crucial role of the carboxyl functionalities of PCA, in coordinating and hence, anchoring the Au NPs onto the surface of the flakes. Indeed, the ATR-FTIR investigation, reported in panel B of Fig. S1 (ESI†), demonstrates that the surface of the RGO flakes is almost deoxygenated by the reduction process from GO.[17]

Fig. 1(B and C) report the Scanning Electron Micrographs (SEM) of the PCA–RGO flakes, collected before and after the decoration with the Au NPs. The surface morphology of the PCA–RGO flakes presents low contrast, sheet like structures (panel B), while for the PCA–RGO/Au NPs samples, a grain-type and bright contrast network of nano-objects onto the sheet like structures, ascribed to the highly electron dense Au NPs, are observed.

Fig. 1(D) shows the UV-Vis absorption spectrum of the hybrid nanocomposite which presents an absorption signal at 564 nm, that can be ascribed to the Localized Surface Plasmon Resonance (LSPR) peak of the Au NPs.[14] Such a band results shifted towards the lower energy side of the spectrum, with respect to the expected position in wavelength of the LSPR from Au NPs of comparable size and shape in solution,[18] likely because of (i) a change of the dielectric constant of the environment of the Au NPs when immobilized onto the aromatic platform of the PCA–RGO flakes, (ii) DMBT mediated electron coupling interactions among the Au NPs immobilized onto the platform,[12] which is made possible considering the high density of the NP coverage,[19] and (iii) PCA and DMBT mediated electron coupling interactions,[4b,5b] and charge transfers at the interface between the Au NPs and the PCA–RGO flakes.[13,20]

Finally, in Fig. 1(E), the Raman spectrum of the PCA–RGO complex is compared with that of the hybrid material. Both the spectra show the typical G and D peaks of RGO. The G peak is related to the bond stretching of all pairs of C-sp^2 atoms in both rings and chains. Conversely, the D peak is due only to the breathing modes of C-sp^2 atoms in rings. The D peak is not visible in the Raman spectrum of perfect graphene, since it derives from a second order Raman process involving the inelastic and elastic scattering of an electron with, respectively, a phonon and a defect. The intense D peak is due to the defects of RGO, eventually comprising ripples, edges, domain boundaries, and/or impurities, which typically can include oxygen containing functionalities, as well as, C heteroatoms and hydrocarbons, in dependence of the synthetic conditions used for the reduction of GO to RGO.[16] As it can be noticed, in the Raman spectrum of the PCA–RGO/Au NP hybrid

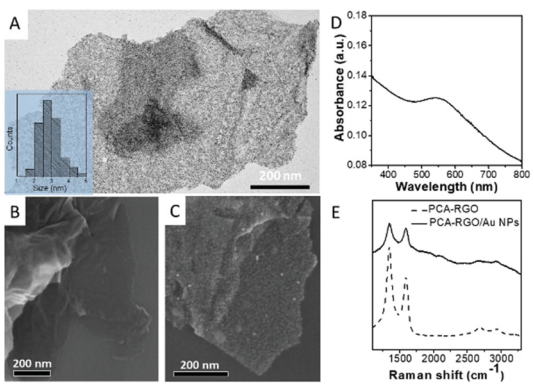

Fig. 1 (A) TEM micrograph of PCA–RGO/Au NPs flakes. SEM images of (B) bare PCA–RGO (160.22×) and (C) PCA–RGO/Au NPs flakes (174.12×), respectively. (D) UV-vis absorption spectrum of 0.15 mg mL^{-1} PCA–RGO/Au NPs flakes, 7×10^{-3} M in Au and 2 mg mL^{-1} in PCA–RGO in toluene. (E) Raman spectra of PCA–RGO and PCA–RGO/Au NPs flakes.

nanocomposite a broad background signal originated from the PCA photoluminescence is observed.[21] In addition, the spectrum of the PCA–RGO/Au NP nanocomposite material shows a lower intensity ratio between the D and G peaks, that is representative of a less defective material, having larger domains of conjugated C-sp^2 atoms,[22] with respect to the PCA–RGO complex. Such an evidence is due to the reduction of the RGO defects which is provided by $NaBH_4$ and occurs at room temperature, because catalyzed by the immobilized Au NPs.[23]

Morphological and electrochemical characterization of the PCA–RGO/Au NPs modified electrodes

Toluene dispersions of the hybrid nanostructures have been drop cast on Screen-Printed Carbon Electrodes (SPCE), fabricated by using the procedure reported in ref. 24 and described in the Experimental section. The SPCEs are planar strips, based on a carbon working electrode (3 mm in diameter), a carbon counter electrode and a silver pseudo-reference electrode.

Fig. 2(A–C) report typical SEM micrographs of the manufactured electrodes, collected at different magnifications. After drop casting the PCA–RGO toluene dispersion, the surface morphology of the electrode appears characterized by the presence of flakes, bright contrast wrinkles and folded edges (Fig. 2(D–F)). Conversely, the surface morphology of the SPCEs after modification with the PCA–RGO/Au NPs hybrid nanocomposite accounts for flakes uniformly coating the surface, and bright grain type structures ascribed to the Au NPs (Fig. 2(G–I)).

The SEM investigation shows the high surface area of the hybrid nanocomposite modified SPCEs, which can be explained by a 2D nanostructure of randomly organized hybrid flakes, where the Au NPs may act as nano-spacers between the stacked PCA–RGO sheets (see Scheme 1), consequently resulting in an increased available surface area.

The SPCEs have been characterized by means of Cyclic Voltammetry (CV) and Electrochemical Impedance Spectroscopy (EIS), before and after their modification. Indeed, these techniques provide relevant information on the kinetic of the electron transfer, the mass transfer regimen at the interface, the electroactive surface area and, therefore, they are frequently used for the evaluation of novel electrode materials.[25]

The CVs of the hybrid modified SPCEs, in 0.5 M H_2SO_4, show a large anodic wave near +1.0 V, along with a cathodic peak at around +0.5 V (Fig. 3(A)), which is ascribed to the oxidation–reduction of Au, thus confirming the presence of the Au NPs available for the electrochemical processes at the electrode surface.

CVs of the SPCEs, either bare and modified with PCA–RGO or PCA–RGO/Au NPs hybrid nanostructures (Fig. 3(B)), have been recorded in presence of $[Fe(CN)_6]^{3-/4-}$, an inner-sphere electroactive redox probe, known to be very sensitive to the surface chemistry and structure of the electrode.

Interestingly, in such a condition, the experiments performed on the PCA–RGO complex and PCA–RGO/Au NPs hybrid modified SPCEs present a decrease of the ΔE_p value with respect to the bare SPCEs, which present the couple of quasi-reversible redox peaks typical of $[Fe(CN)_6]^{3-/4-}$ (Fig. 3(B)). This evidence accounts for the higher conductivity and for the enhancement of the electron transfer capability at the electrode/electrolyte interface, upon the SPCE surface modification. In addition, the peak current of the PCA–RGO/Au NPs hybrid modified SPCEs increases with respect to that of the bare and of the PCA–RGO modified SPCEs (Fig. 3(B)), reasonably for the

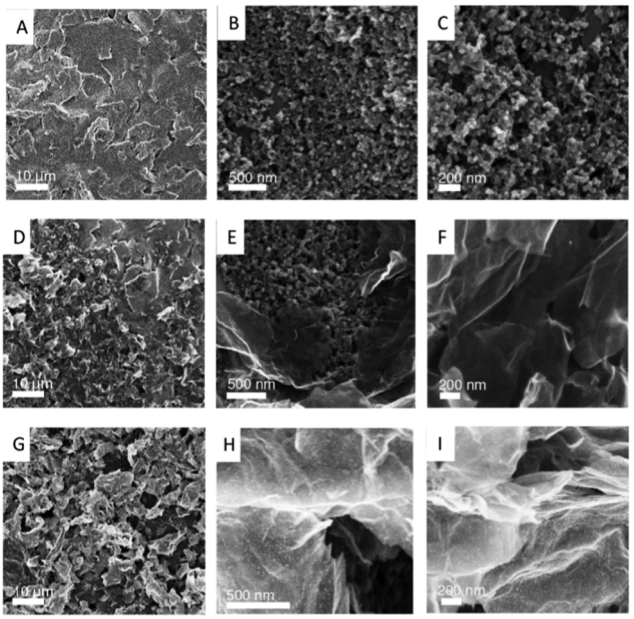

Fig. 2 SEM micrographs of SPCEs as bare (A–C), and coated by PCA–RGO (D–F) and PCA–RGO/Au NPs flakes (G–I), recorded at 5 kV and three increasing magnifications (1.65k× (A), 41.78k× (B), 102.16k× (C), 1.81k× (D), 42k× (E), 101.67k× (F), 1.64k× (G), 42.93k× (H) and 123k× (I)).

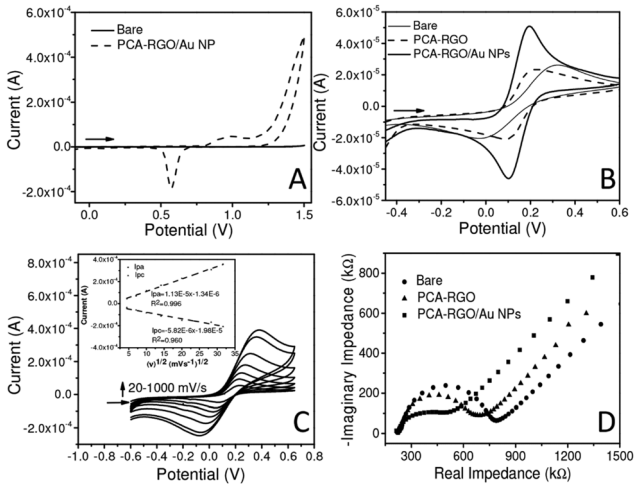

Fig. 3 CVs of SPCEs, (A) as bare (solid curve) and modified with the PCA–RGO/Au NPs hybrid nanocomposite in 0.5 M H_2SO_4 at 10 mV s^{-1} (dashed curve), (B) as bare and modified by PCA–RGO and PCA–RGO/Au NPs in 0.1 M KCl and 5 mM $[Fe(CN)_6]^{3-/4-}$ at 10 mV s^{-1}, (C) modified by PCA–RGO/Au NPs at different scan rates in 0.1 M KCl and 5 mM $[Fe(CN)_6]^{3-/4-}$. (inset of C) Plots of the anodic (I_{ap}) and cathodic (I_{cp}) peak currents *vs.* square root of scan rate ($\nu^{1/2}$). (D) EIS spectra (Nyquist plots) before (●) and after SPCE modification with (▲) PCA–RGO and (■) PCA–RGO/Au NPs in 5 mM $[Fe(CN)_6]^{3-/4-}$ and 0.1 M KCl.

increase of the electroactive surface area, attesting for the higher electrochemical reactivity of the hybrid modified SPCEs.

The values of the electroactive area (A_{ele}) (Table S1 of the ESI†) of both the bare and PCA–RGO/Au NPs modified SPCEs have been estimated by using the Randles–Sevcik equation reported in eqn (1) of the Experimental section. The A_{ele} value of the PCA–RGO/Au NPs modified SPCEs, namely 14 ± 2 mm^2, almost doubles, in comparison with the geometric area of the SPCE (7 mm^2).

The apparent heterogeneous electron transfer rate constant (k_0), which is intrinsically dependent on ΔE_p values (where a smaller ΔE_p value corresponds to a high reversibility of the redox probe, and thus, to faster heterogeneous electron transfer (ET) kinetics for a given electrode material), has been calculated, by using the Nicholson method,[26] for quasi-reversible systems (Table S1 of the ESI†). The k_0 value, namely $9.3 \pm 0.7 \times 10^{-4}$ cm s^{-1}, obtained for the hybrid nanocomposite modified SPCE, is threefold higher than that of the bare SPCEs, that is $2.7 \pm 0.5 \times 10^{-4}$ cm s^{-1}, thus indicating that the hybrid nanostructures modification results in an increased conductivity and faster heterogeneous electron transfer kinetics at the electrode surface.

The voltammetry peak intensity (I_p) has been monitored as a function of the scan rate (ν), from 20 to 1000 mV s^{-1} (inset of Fig. 3(C)) and the linearity of the plots, of both the anodic and cathodic peak currents, reported *versus* the square root of the scan rate, confirms the diffusion-controlled electron transfer.

EIS has been used to further characterize the modified electrode surface (Fig. 3(D)). The impedance spectra, reported as Nyquist plots, include a semicircle portion at higher frequencies, where the diameter of the semi-circle corresponds to the electron transfer resistance (R_{et}) at the electrode interface and a linear portion at lower frequencies, which represents the diffusion process. In particular, a R_{et} of *ca.* 0.5 ± 0.1 kΩ can be estimated for the bare SPCEs, a R_{et} of *ca.* 0.4 ± 0.1 kΩ for the PCA–RGO modified SPCEs, and a much lower resistance of *ca.* 0.30 ± 0.08 kΩ is measured for the electrode modified with the PCA–RGO/Au NPs hybrid flakes.

This finding can be reasonably accounted for by the high surface area of the hybrid nanostructures modifying the SPCE, as well as, the excellent electrical conductivity of the PCA–RGO/Au NPs hybrid nanocomposite, since it accelerates the electron transfer at the electrode/electrolyte interface, thus confirming the indication provided by the CV results.

The electrochemical behaviour of the PCA–RGO/Au NPs hybrid modified SPCEs has been first assessed towards selected reagents of electrochemical enzyme-catalyzed assays, namely 1-naphthol, tetramethylbenzidine (TMB) and H_2O_2, that are produced by the reaction catalyzed by Alkaline Phosphatase (AP), Horse Radish Peroxidase (HRP) and Glucose Oxidase (GOD), respectively. The results, reported in Fig. S2 and S3 of the ESI,† indicate an enhanced detection of the oxidized TMB product (TMBox) and H_2O_2. Such features can be ascribed to the combination of the high charge mobility and of the charge sink properties of RGO, the high surface area and high electroactivity of the Au NPs, which synergistically contribute to improve the electron transfer kinetics, and the electrocatalytic activity of the electrodes, towards TMBox reduction and H_2O_2 oxidation. The PCA–RGO/Au NPs modified SPCE may then offer an ideal platform for developing peroxidase- and oxidase-based electrochemical biosensors.

AP is a very popular enzyme that may be exploited for a wide range of bioassays, due to the intrinsic simplicity of the approach, based on the detection of one compound that allows conversion of a redox-inactive reagent, into a redox-detectable product. On the other hand, 1-naphthyl phosphate is one of the most used substrate of AP and it is converted in 1-naphthol by enzymatic hydrolysis.[27] Thus, CV has been used to assess the electrochemical performance of the PCA–RGO/Au NPs modified SPCEs in presence of 1-naphthol. CV scans of a 500 μM solution of 1-naphthol, in di-ethanol amine buffer (DEA) at pH 9.6, have been performed on both PCA–RGO/Au NPs modified and unmodified SPCEs and bare screen-printed Au electrodes (SPGE), in the potential range of −0.2 to +0.6 V (Fig. 4(A)), keeping constant the geometrical area of the electrode (7 mm^2).

The PCA–RGO/Au NPs modified SPCEs exhibit the largest current response, being about 1.5 and 3 times higher than those recorded for unmodified SPCEs and SPGEs, respectively, with a potential negatively shifted with respect to the bare SPCEs (about 20 mV) and SPGEs (about 100 mV) and a response time lower than 20 s (Fig. 4(A)). During the reverse scan, no cathodic peak is observed for 1-naphthol, pointing out the irreversibility of its oxidation process.[27] The PCA–RGO/Au NPs hybrid modified SPCEs clearly favour the 1-naphthol oxidation, as evident from the increase of the anodic peak current, and decrease of the overpotential, when compared to the bare SPCEs and SPGEs. Thus, the PCA–RGO/Au NPs modified SPCEs have been proved efficient electrocatalyst for accomplishing a sensitive determination of 1-naphthol.

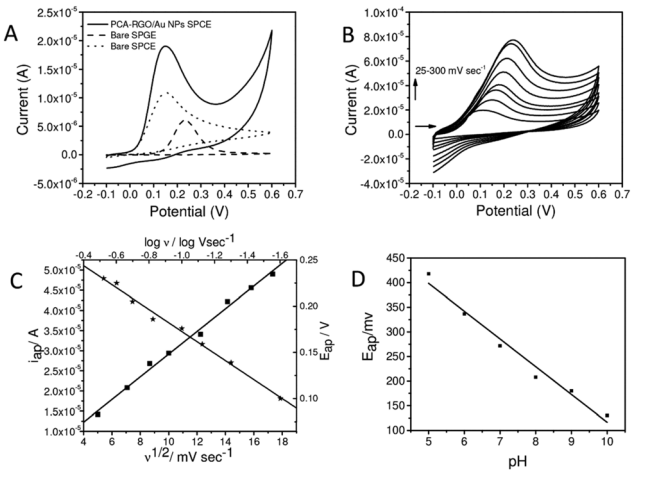

Fig. 4 (A) CVs of 500 μM 1-naphthol at PCA–RGO/Au NPs SPCEs, bare SPCEs, SPGEs in DEA buffer 0.1 M at pH 9.6 and scan rate of 50 mV s^{-1}. (B) CVs of 500 μM 1-naphthol at PCA–RGO/Au NPs SPCEs with different scan rates, from 0.025 to 0.300 V s^{-1}. (C) Plot of i_{ap} of *B vs.* $\nu^{1/2}$ and plot of E_{ap} of 1-naphthol *vs.* log ν. (D) Plot of the E_{ap} *vs.* the pH obtained from CVs of 200 μM 1-naphthol in 0.1 M phosphate solution containing 0.1 M KCl supporting electrolyte, in the −0.2 to +0.8 V potential range, at the scan rate of 50 mV s^{-1}.

Then, charge transport characteristics at the modified electrodes have been investigated by means of CV by performing runs at increasing scan rates (ν) (Fig. 4(B)). The oxidation peak potential has been found to shift towards more positive values when the scan rate is increased, indicating the kinetic limitation of the electrochemical reaction. The proportional relationship of the logarithm of the scan rate ($\log \nu$) *vs.* the anodic peak potential (E_{ap}) reported in Fig. 4(C), confirms the irreversibility of the redox process, as the slope is greater than 30 mV per tens.[28] Meanwhile, the plot of the peak current (i_{ap}) *vs.* the square root of the scan rate ($\nu^{1/2}$) can be fitted by linear regression, indicating a diffusion-controlled electrochemical process (Fig. 4(C)).

A series of CV runs for the 200 μM 1-naphthol in 0.1 M phosphate solution, containing 0.1 M KCl (as supporting electrolyte), at different pH, over the potential −0.2 to +0.8 V, and with a scan rate of 50 mV s^{-1} (Fig. 4 – panel D), shows that the oxidation peak potential moves to lower values with increasing the solution pH, indicating the involvement of protons in the electrochemical reaction. The plot of E_{ap} *vs.* pH shows a linear trend, fitted by using the equation $E_{ap} = -56$ pH + 680, characterized by a slope close to the theoretical value derived from Nernst equation, suggesting that the oxidation process removes one proton per electron.

Differential pulse voltammetry (DPV) experiments performed on 1-naphthol, in DEA buffer at pH 9.6, have resulted in a defined oxidation peak (data not shown), and a linear behaviour has been observed in the investigated concentration range (0.001–0.2 mM). A LOD of 0.2 μM (S/N = 3), corresponding to 1 nmol in 150 μl, has been obtained. Considering that 1 unit of enzyme is able to convert 1 μmol min^{-1} of substrate, the PCA–RGO/Au NPs hybrid modified SPCEs appear useful in the detection of low levels of enzyme. Good reproducibility has been observed for a concentration of 0.2 mM of 1-naphthol in DEA buffer, with a % RSD of 8% ($n = 5$). Therefore, the hybrid modified SPCEs can effectively be used for the highly sensitive determination of enzymatically generated 1-naphthol, in an enzymatic amplified electrochemical bioassay.

Electrochemical genosensing experiments

Scheme 2 reports a sketch of the proposed enzyme amplified genosensor assay. The DNA CP has been immobilized on the Au NPs surface of the hybrid modified SPCEs, *via* Au–thiol binding. The chemisorption of thiolated DNA capture probes (CPs) onto the metal surface leads to the formation of self-organized layers that are subsequently backfilled with a second shorter alkanethiol, namely 6-mercapto-1 hexanol (MCH). This treatment aims to remove any competing nonspecific adsorption of other species and favours the organization of the DNA strand[29] onto the nanoscale domains provided by the Au NP surface, so that they result not too closely packed, ultimately limiting steric hindrance and electrostatic repulsion during the hybridization with the miRNA-221 target. Preliminary genosensing results indicate the good stability of PCA–RGO/Au NPs hybrid sensors modified with the mixed monolayer of thiolated probes and MCH. This allows serial preparation of many sensors that can be stored until use. Effect of aging time on the selectivity and sensitivity of the genosensors are still under investigation.

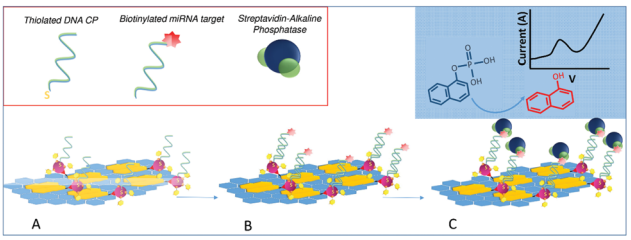

Scheme 2 Sketch of the preparation of the PCA–RGO/Au NPs modified SPCEs for the electrochemical genosensor assay. (A) Immobilization of the DNA CP on the PCA–RGO/Au NPs modified SPCEs. (B) Hybridization of the DNA CP with miRNA-221 target. (C) Exposure of the SPCEs to AP, incubation of the substrate in 1-naphthyl phosphate, generation of 1-naphthol detected by DPV.

The DNA CP-functionalized hybrid modified SPCEs have been let to react with the miRNA-221, and subsequently, they have been exposed to streptavidin–alkaline phosphatase (AP). After incubation in the 1-naphthyl phosphate substrate, the production of 1-naphthol, catalyzed by AP, has been detected by monitoring its oxidation peak current by DPV.

The electron transfer resistance of the genosensor has been investigated by EIS after each fabrication step, starting from the hybrid nanostructures modified SPCEs. Fig. 5(A) displays the Nyquist plots of the PCA–RGO/Au NPs SPCEs, before and after modification with CP (PCA–RGO/AuNPs/CP), and after hybridization with the 10 nM solution of the target (T) miRNA-221 strand (PCA–RGO/AuNP/CP/T).

The plot concerning the PCA–RGO/Au NPs modified SPCEs is semicircular in shape, having a R_{et} of about 0.30 ± 0.08 kΩ, which increases up to 0.6 ± 0.1 kΩ after CP immobilization (Fig. 5(A)), due to the repulsion of the $[Fe(CN)_6]^{3-/4-}$, caused by the negatively charged phosphoric acid backbones of the CPs, ultimately inhibiting electron transfer. An enhancement of the R_{et} up to 1.2 ± 0.2 kΩ is observed after the hybridization of DNA-CP with the 10 nM solution of the target miRNA-221, due to an increase of the negative charge, originated from the double-stranded RNA/DNA formation.

The analytical performance of the modified SPCEs in the assay has been estimated by performing a calibration experiment. The current has been found to increase with the target miRNA-221 concentration, from 1 pM to 5 nM (Fig. 5(B)) and

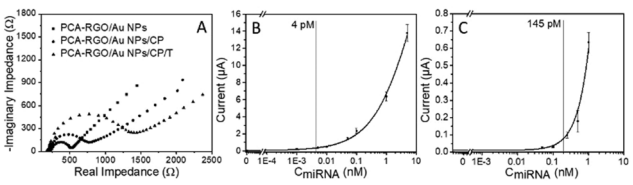

Fig. 5 (A) Faradaic impedance spectra (in form of Nyquist plots) in 0.1 M KCl and 5 mM $[Fe(CN)_6]^{3-/4-}$ (1 : 1) solution of (■) PCA–RGO/Au NPs SPCEs, (●) DNA CP functionalized SPCEs (PCA–RGO/AuNPs/CP) and (▲) PCA–RGO/AuNPs/CP SPCEs after incubation with the 10 nM miRNA-221 target (PCA–RGO/Au NPs/CP/T). In (B and C) miRNA-221 calibration plots in PB, achieved by PCA–RGO/AuNPs SPCEs (B) and bare SPGEs (C). (B and C) The error bar corresponds to the standard deviation and the vertical bar points at the minimum concentrated detected value.

the LOD has been determined to be 0.7 pM (0.7 amol in 10 μL), considering the detection limit as the value of the background signal added of three times its standard deviation. The limit of quantification (LOQ), defined as the background signal, plus ten times its standard deviation, has been evaluated to be 4 pM (Fig. 5(B)). A relative standard deviation of 16% (expressed as the mean of all concentrations tested) has been obtained. When compared to bare SPGEs of the same geometrical area, the PCA–RGO/Au NPs hybrid modified SPCEs have shown better performance in the lower end of the concentration range. A LOD and LOQ of 33 pM and 145 pM, respectively, have been estimated for the bare SPGEs. The LOQ has been found a factor of *ca.* 40 lower for the PCA–RGO/Au NPs hybrid modified SPCEs than for the bare SPGEs (Fig. 5(C)).

The PCA–RGO/Au NPs hybrid modified SPCEs have been then demonstrated to significantly improve the sensitivity of the assay, obtaining for the minimum detected concentration, a value 50 times lower than that recorded with the hybrid modified SPGEs (Fig. 5(C)).

The LOD value of the proposed system (0.7 pM) has been found lower than other LOD values recently reported, still using AP as enzymatic label and graphene–AuNPs nanocomposites as electrode modifiers (see Table S2 of the ESI†) and comparable with the values reported for other electrochemical methods for miRNA analysis.[13b]

The enhanced analytical performance of the hybrid nanostructures modified SPCEs are ascribed to the high conductivity of the proposed hybrid nanocomposite modified electrodes, the fast electron transfer kinetics, the high electroactivity of the electrode towards 1-naphthol oxidation and the high electroactive area and morphology[30] of the nanostructured surface.

Indeed, such a morphology offers convenient geometry for the hybridization process, providing a high extent of the DNA CP immobilization, and hence amplified hybridization events with the miRNA target.[4]

The operational reliability and feasibility of the developed voltammetric genosensor has been finally assessed. Spiked samples, prepared by adding different concentrations of miRNA-221 to diluted human blood serum samples, namely 10 and 100 pM (Fig. S4, ESI†), were analyzed, and the recovery was demonstrated, though the values determined, 103% and 117%, respectively, were affected by unspecific physisorption of serum proteins at the electrode surface. Overall, the feasibility of the proposed assay for the determination of miRNA-221 in real biological samples can be safely inferred.

Conclusions

Novel colloidal hybrid nanostructures formed of pyrenecarboxylic acid (PCA) surface modified RGO flakes, highly densely coated by a uniform network of thiol-capped Au NPs, PCA–RGO/Au NPs, have been synthesized. The NPs growth, proceeding by an *in situ* colloidal reduction of an Au precursor, in presence of DMBT and of $NaBH_4$, results in a high control on the NP size and size distribution, notably, on the overall nanostructured morphology of the final decorated PCA–RGO flakes, since the aromatic thiol favors the π–π induced Au NP stacking into assemblies onto the PCA–RGO platform, concomitantly enabling electron coupling interactions among the Au NPs. Moreover, PCA acts as linker and coupling agent between the RGO flakes and the Au NPs, thanks to the π–π interactions of its aromatic structure with the RGO platform and, concomitantly to its carboxyl moieties, serving as coordinating active sites for the Au NPs.

These hybrid nanostructures have been applied for the modification of the SPCEs, resulting in electrodes with an increased electroactive surface area, a higher electrical conductivity, a faster heterogeneous electron transfer kinetics at the electrode interface, with an higher electron transfer constant ($K_0 = 9.3 \pm 0.7 \times 10^{-4}$ cm s^{-1}) and a decreased resistance at the electrode–electrolyte interface (R_{et} = 0.30 ± 0.08 kΩ) with respect to the PCA–RGO and pristine SPCEs.

The manufactured colloidal hybrid modified SPCEs have demonstrated a well-suited platform for developing AP-, HRP- and GOD-based electrochemical biosensors for enzyme amplified bioassays. In particular, the platform has been found highly reliable and sensitive in the AP mediated signal amplification based assay of the miRNA-221 biomarker, detected in spiked human blood serum samples, with a LOD of 0.7 pM (7 amol in 10 μL) and an average percentage standard deviation (RSD) of 13% in a range of 1–5000 pM.

Overall, the proposed hybrid nanostructures modified electrodes hold a great promise in amplifying the transducer sensitivity, opening the venue to the development of new affinity assays for the detection of other oligonucleotides and biomolecules, with an improved sensitivity that could be effectively developed in cost efficient and sensitive detection systems to be potentially implemented in point of care devices.

Experimental section

Materials

Commercial RGO (1.6 nm flakes) was purchased from Graphene Supermarket. 1-Pyrenecarboxylic acid (PCA, 97%), *n*-methyl-2-pyrrolidone (NMP, 99%), tetraoctylammonium bromide (TOAB, 99%), hydrogen tetrachloroaurate(III) trihydrate ($HAuCl_4 \times 3H_2O$, 99.999%), 3,4-dimethylbenzenethiol (DMBT, 98%), 2-phenylethanethiol (98%), sodium borohydride ($NaBH_4$, 99.99%), toluene, methanol, tris(2-carboxyethyl)phosphine (TCEP), 6-mercapto-1-hexanol (MCH), streptavidin–alkaline phosphatase (S2890, Strept–AP, 2 : 1 conjugation stoichiometry), diethylpyrocarbonate (DEPC), Tris–HCl, 1-naphthyl phosphate, bovine serum albumin (BSA), diethanolamine (DEA) and human serum type AB were obtained from Sigma-Aldrich. Tetramethylbenzidine (TMB) was purchased from Abraxis. 0.45 μm polyethylene sulphone (PES) syringe filter were obtained from Sarstedt. Disodium hydrogenphosphate, potassium hexacyanoferrate (III and II), sulphuric acid, magnesium and potassium chloride were purchased from Merck. NAP-10 columns of Sephadex G-25 were obtained from GE Healthcare. MilliQ water (DEPC treated for RNA analysis) was used throughout the experimental work.

Synthetic oligonucleotides, namely Probe (DNA-SH, 5′-GAA-ACC-CAG-CAG-ACAATG-TAG-CT-SH 3′) and Target (5′-AGC-UAC-AUU-GUC-UGC-UGG-GUUUC-biotin 3′) were purchased from MWG Biotech AG. The target sequence, corresponding to the mature miRNA-221, that is a mi-RNA sequence overexpressed in lung and breast cancers, was chosen as model oligonucleotide. The small RNA can be terminal conjugated with biotin following the label procedure reported recently in ref. 31.

Prior to use, the DNA-SH probes were treated with TCEP. This reagent allows reduction and cleavage of oligo dimers eventually obtained by oxidative coupling of two DNA-SH molecules (*i.e.* DNA-SS-DNA). The lyophilized oligonucleotides were dissolved in a 10 mM Tris–HCl buffer solution (pH 8.3) containing 10 mM of TCEP. The reaction was allowed to proceed for 1 hour at room temperature. The thiolated DNA was then purified by elution through a NAP-10 column of Sephadex G-25 by using 100 μM Tris buffer, containing 1 μM EDTA. DNA-SH stock solutions were prepared in the same buffer and stored frozen.

Synthesis of the PCA–RGO/Au NPs hybrid material. For the preparation of the PCA–RGO/Au NPs hybrid material, a two-phase method, used for the synthesis of Au NPs of M. Brust *et al.*[14] was followed, with minor modifications. In a typical experiment, 15 mg of the PCA modified RGO powder were dissolved in a solution prepared by mixing 1.1872 g of TOAB in 35 mL of toluene, and left to stir 30 min. To this solution, 0.1770 g of $HAuCl_4 \times 3H_2O$, dispersed in 15 mL of milliQ water, were added and left to stir 30 min. After transfer of the Au precursor from water to toluene, which is assisted by TOAB, water was removed from the reaction flask, and 60 μl of DMBT were added, for allowing controlled reduction of Au(III) to Au(I), and left to stir for 1 hour. Finally, 0.1892 g of $NaBH_4$ in 12 mL of MilliQ water were added, and the growth of the Au NPs was allowed to proceed overnight. The PCA–RGO/Au NPs dispersions were then purified with methanol by cycles of centrifugation to remove the excess of the DMBT aromatic ligand. Finally, a separation procedure has been carried out to separate homonucleated Au NPs from the PCA–RGO/Au NPs hybrid flakes, by means of a cycle of centrifuge upon addition of methanol. The isolated pellet containing the hybrid flakes was then re-dispersed in toluene for the spectroscopic and morphological characterization.

Fabrication of the PCA–RGO/Au NPs modified electrodes. With the exception of carbon screen-printed ink (that was obtained from DuPont, Italy), materials and procedures to screen-print the electrode transducers are described in previously published papers.[24,32] Screen-printed carbon electrodes (SPCEs) are a three electrode electrochemical cell, constituted by a graphite working electrode ($\varnothing$ = 3.0 mm, A_{geom} = 7 mm^2), a silver pseudo-reference electrode and a graphite counter electrode. Screen-printed Au electrodes (SPGEs) are three electrode electrochemical cells, constituted by an Au working electrode ($\varnothing$ = 3.0 mm, A_{geom} = 7 mm^2), a silver pseudo-reference electrode and a graphite counter electrode. The SPCEs and SPGEs were modified by drop-casting 1 μL of the PCA–RGO/Au NPs suspensions on the electrode surface.

Hybridization assay. SPCEs surface modified with PCA–RGO/Au NPs as well as SPGEs were exposed to the capture probe (CP), namely 10 μL of 0.1 μM DNA-SH in 0.5 M phosphate buffer solution at pH 7.4. Chemisorption onto the electrodes was allowed to proceed overnight, for 16 hours, storing the electrodes in a Petri dish for preventing the solution to evaporate. Then, 8 μL of a 1 mM aqueous solution of MCH was placed onto the probe-modified surface for 30 min for the voltammetric investigation. In the case of EIS measurements, the MCH concentration was 0.1 mM. Prior to the hybridization reaction, the PCA–RGO/AuNP/CP modified SPCEs as well as CP modified SPGEs were washed twice with 15 μL of 0.5 M phosphate buffer at pH 7.4.

Hybridization experiments were carried out by using the biotinylated target miRNA-221 sequence in a direct assay format.[30c] CP modified electrodes, were exposed for 20 min to 8 μL of the biotinylated target sequence in 0.5 M phosphate buffer solution at pH 7.4. After hybridization, the sensors were washed three times with 15 μL of DEA buffer solution, 0.1 M in diethanolamine, 1 mM in $MgCl_2$ and 100 mM in KCl at pH 9.6.

The biotinylated hybrid obtained at the electrode surface was reacted with 8 μL of a solution containing 0.8 U mL^{-1} of the streptavidin–alkaline phosphatase conjugate and 10 mg mL^{-1} of BSA blocking agent in DEA buffer.

After 20 min, the sensors were washed three times with 15 μL of DEA buffer. The planar electrochemical cell was then incubated with 150 μL of a 1 mg mL^{-1} 1-naphthyl phosphate solution in DEA buffer. The 1-naphthol oxidation peak was taken as the analytical signal. After 20 min, the electrochemical signal of the enzymatically produced 1-naphthol was measured by DPV with a modulation time of 0.05 s, an interval time of 0.15 s, a step potential of 5 mV, a modulation amplitude of 70 mV and a potential scan between 0 to 600 mV. All the results are reported as the mean value of at least three measurements and the error bars correspond to the standard deviation.

Human serum spiked samples. Human serum type AB was diluted 1 : 100 (v/v) in phosphate buffer (PB) and filtered by a 0.45 μm pore filter in polyethersulfone (PES). Spiked samples were prepared by adding known quantities (10 and 100 nM) of miRNA-221 to diluted serum.

Characterization techniques. Steady state UV-Vis absorption spectroscopic properties of the PCA–RGO/Au NPs hybrid material were investigated by means of a Cary 5000 (Varian) UV/Vis/NIR spectrophotometer, at room temperature. Steady state photoluminescence (PL) spectra were recorded by using a Fluorolog 3 spectrofluorometer (HORIBA Jobin-Yvon), equipped with double grating excitation and emission monochromators. All optical measurements were performed at room temperature.

Raman spectra were collected by using a LabRAM HR Horiba-Jobin Yvon spectrometer with a 532 nm excitation laser source. Measurements were carried out under ambient conditions at a low laser power (1 mW) to avoid laser-induced damage of the sample. The Raman band recorded from a silicon wafer at 520 cm^{-1} was used to calibrate the spectrometer, and accuracy of the spectral measurement was estimated to be 1 cm^{-1}.

Mid-infrared spectra were acquired with a Varian 670-IR spectrometer equipped with a DTGS (deuterated triglycine sulfate) detector. The spectral resolution used for all experiments

was 4 cm^{-1}. For attenuated total reflection (ATR) measurements, the internal reflection element (IRE) used was a one-bounce 2 mm diameter diamond microprism. Cast films have been prepared directly onto the internal reflection element, by depositing the solution or suspension of interest on the upper face of the diamond crystal and allowing the solvent to evaporate.

Transmission Electron Microscopy (TEM) analyses were performed by using a Jeol Jem-1011 microscope, operating at 100 kV and equipped by a high-contrast objective lens, a W filament as electron source, and an ultimate point resolution of 0.34 nm. Images were acquired by a Quemesa Olympus CCD 11 Mp Camera. Samples were prepared by dipping a 300 mesh amorphous carbon-coated Cu grid in toluene dispersions of the PCA–RGO/Au NPs and leaving the solvent to dry. Size statistical analyses of the NP average size and size distribution were performed by counting 200 nanoparticles by the freeware ImageJ analysis program.

Field emission scanning electron microscopy (FE-SEM) was performed by a Zeiss Sigma microscope, operating in the range of 0–10 keV, and equipped with an in-lens secondary electron detector and an INCA Energy Dispersive Spectroscopy (EDS) detector. Samples were mounted onto stainless-steel sample holders by double-sided carbon tape and grounded by silver paste.

Topography and phase mode Atomic Force Microscopy (AFM) measurements were performed in air and at room temperature, by means of a PSIA XE-100 SPM system operating in tapping mode. A silicon Scanning Probe Microscope (SPM) sensor for noncontact AFM (Park Systems), having a spring constant of 42 N m^{-1} and a resonance frequency of 330 kHz, was used. Micrographs were collected on six distinct areas of the sample, with a scan size area of 5 μm × 5 μm, by sampling the surface at a scan rate between 1.0–0.5 Hz and a resolution of 256 × 256 pixels. Topography AFM images were processed by using XEI software to obtain statistical data.

Electrochemical measurements. The electrochemical measurements were carried out at room temperature (25 °C), with a three-electrode system, and an AUTOLAB PGSTAT 10 digital potentiostat/galvanostat. The GPES 4.9004 software (Eco Chemie BV, Utrecht, The Netherlands) was used for Cyclic Voltammetry (CV), Differential Pulse Voltammetry (DPV), Amperometry and Multi-Pulse Amperometry (MPA). The FRA2 module was used for faradaic impedance experiments. All potentials were referred to the screen-printed silver pseudo-reference electrode and the experiments were carried out at room temperature.

CV was performed by a planar electrochemical cell covered by 150 μL of an electrolyte solution. When $Fe[(CN)_6]^{3/4-}$ in 0.1 M KCl was used as redox probe, the potential was scanned from −0.6 V to +0.65 V *vs.* the Ag/AgCl pseudo-reference electrode. When a solution containing 0.5 M of H_2SO_4 was used, the potential was scanned from −0.6 V to +1.5 V, with a scan rate of 10 mV s^{-1}.

The electroactive areas (A_{ele}) have been determined by using the Randles–Sevcik equation for a quasi-reversible system:

$$I_{ap} = (2.69 \times 10^5) A_{ele} C D^{1/2} n^{3/2} \nu^{1/2} \quad (1)$$

where I_{ap} is the anodic peak current, D is the diffusion coefficient of $[Fe(CN)_6]^{4-}$ in solution (6.5×10^{-6} cm^2 s^{-1}), n is the number of electrons transferred in the redox reaction, ν is the potential scan rate (V s^{-1}) and C is the $[Fe(CN)_6]^{4-}$ concentration in the bulk solution (mol cm^{-3}).

The amperometric measurements for H_2O_2 detection were performed at an applied potential of +0.65 V *vs.* the Ag/AgCl pseudo-reference electrode, in 0.05 M phosphate buffer at pH 8.5, under stirring.

Faradaic impedance measurements were carried out in the presence of 5 mM $[Fe(CN)_6]^{3/4-}$ redox probe (equimolecular mixture in 0.1 M KCl). A sinusoidal voltage of 10 mV in amplitude (peak-to-peak), within the frequency range of 100 kHz–10 mHz, was superimposed to the applied bias potential. The dc potential was set up at the potential value observed at the Open Circuit Potential (O.C.P.) before each measurement. Experimental spectra, presented in the form of complex plane diagrams (*i.e.* Nyquist plots), were fitted with proper equivalent circuits by using the FRA2 software 4.9004 (EcoChemie). Charge transfer resistance values were taken as analytical signals. The Randles equivalent circuit was successfully applied to fit the acquired data.

Conflicts of interest

There are no conflicts to declare.

Acknowledgements

This work was supported by the National Project (PRIN 2012 prot. 20128ZZS2H).

Notes and references

1 (*a*) H. Dvinge, A. Git, S. Gräf, M. Salmon-Divon, C. Curtis, A. Sottoriva, Y. Zhao, M. Hirst, J. Armisen, E. A. Miska, S. F. Chin, E. Provenzano, G. Turashvili, A. Green, I. Ellis, S. Aparicio and C. Caldas, *Nature*, 2013, **497**, 378; (*b*) L. Manterola, E. Guruceaga, J. G. Perez-Larraya, M. Gonzalez-Huarriz, P. Jauregui, S. Tejada, R. Diez-Valle, V. Segura, N. Sampron, C. Barrena, I. Ruiz, A. Agirre, A. Ayuso, J. Rodrıguez, A. Gonzalez, E. Xipell, A. Matheu, A. Lopez de Munain, T. Tunon, I. Zazpe, J. Garcıa-Foncillas, S. Paris, J. Y. Delattre and M. M. Alonso, *Neurooncology*, 2014, **16**, 520.

2 S. Chakraborty and C. R. Raj, *Biosens. Bioelectron.*, 2009, **24**, 3264.

3 (*a*) F. Bonaccorso, Z. Sun, T. Hasan and A. C. Ferrari, *Nat. Photonics*, 2010, **4**, 611; (*b*) O. V. Yazyev and Y. P. Chen, *Nat. Nanotechnol.*, 2014, **9**, 755; (*c*) E. Morales-Narváez, L. Baptista-Pires, A. Zamora-Gálvez and A. Merkoçi, *Adv. Mater.*, 2016, **29**, 1604905; (*d*) B. Wu, N. Zhao, S. Hou and C. Zhang, *Nanomaterials*, 2016, **6**, 220.

4 (*a*) K. Turcheniuk, R. Boukherroub and S. Szunerits, *J. Mater. Chem. B*, 2015, **3**, 4301; (*b*) X. Chen, L. Wang, S. Sheng, T. Wang, J. Yan, G. Xie and W. Feng, *Anal. Chim. Acta*, 2015, **889**, 90; (*c*) I. Tiwari, M. Gupta, C. M. Pandey and

V. Mishra, *Dalton Trans.*, 2015, **44**, 15557; (*d*) A. Bonanni, A. Ambrosi and M. Pumera, *Chem. – Eur. J.*, 2012, **18**, 4541.
5 (*a*) Q. Chen, L. Zhang and G. Chen, *Anal. Chem.*, 2012, **84**, 171; (*b*) Y. Zhang, X. Bai, X. Wang, K.-K. Shiu, Y. Zhu and H. Jiang, *Anal. Chem.*, 2014, **86**, 9459.
6 H.-P. Peng, Y. Hu, P. Liu, Y.-N. Deng, P. Wang, W. Chen, A.-L. Liu, Y.-Z. Chen and X.-H. Lin, *Sens. Actuators, B*, 2015, **207**, 269.
7 T. Kilic, A. Erdem, M. Ozsoz and S. Carrara, *Biosens. Bioelectron.*, 2018, **99**, 525.
8 C. Ingrosso, G. V. Bianco, V. Pifferi, P. Guffanti, F. Petronella, R. Comparelli, A. Agostiano, M. Striccoli, I. Palchetti, L. Falciola, M. L. Curri and G. Bruno, *J. Mater. Chem. A*, 2017, **5**, 9307.
9 K. S. Novoselov, V. I. Falko, L. Colombo, P. R. Gellert, M. G. Schwab and K. Kim, *Nature*, 2012, **490**, 192.
10 C. Ingrosso, G. V. Bianco, M. Corricelli, R. Comparelli, D. Altamura, A. Agostiano, M. Striccoli, M. Losurdo, M. L. Curri and G. Bruno, *ACS Appl. Mater. Interfaces*, 2015, **7**, 4151.
11 V. Georgakilas, M. A. Otyepka, A. B. Bourlinos, V. Chandra, N. Kim, K. C. Kemp, P. Hobza, R. Zboril and K. S. Kim, *Chem. Rev.*, 2012, **112**, 6156.
12 S. Pradhan, D. Ghosh, L.-P. Xu and S. Chen, *J. Am. Chem. Soc.*, 2007, **129**, 10622.
13 (*a*) Y. Du, S. Guo, S. Dong and E. Wang, *Biomaterials*, 2011, **32**, 8584–8592; (*b*) S. Campuzano, R. M. Torrente-Rodríguez, E. López-Hernández, F. Conzuelo, R. Granados, J. M. Sánchez-Puelles and J. M. Pingarrón, *Angew. Chem., Int. Ed.*, 2014, **53**, 6168; (*c*) D. Kong, S. Bi, Z. Wang, J. Xia and F. Zhang, *Anal. Chem.*, 2016, **88**, 10667; (*d*) F. Bettazzi, S. Laschi, D. Voccia, A. Testolin, C. Gellini, G. Pietraperzia, L. Falciola, V. Pifferi, C. Ingrosso, T. Placido, R. Comparelli, M. L. Curri and I. Palchetti, *Electrochim. Acta*, 2018, **276**, 389.
14 (*a*) M. Brust, M. Walker, D. Bethell, D. J. Schiffrin and R. Whyman, *J. Chem. Soc., Chem. Commun.*, 1994, 801; (*b*) M. Zhu, E. Lanni, N. Garg, M. E. Bier and R. Jin, *J. Am. Chem. Soc.*, 2008, **130**, 1138.
15 G. Goncalves, P. A. A. P. Marques, C. M. Granadeiro, H. I. S. Nogueira, M. K. Singh and J. Gracio, *Chem. Mater.*, 2009, **21**, 4796.
16 (*a*) A. Ferrari, *Solid State Commun.*, 2007, **143**, 47; (*b*) C. K. Chua and M. Pumera, *Chem. Soc. Rev.*, 2014, **43**, 291.
17 H. Zhang, D. Hines and D. L. Akins, *Dalton Trans.*, 2014, **43**, 2670.
18 M. C. Daniel and D. Astruc, *Chem. Rev.*, 2004, **104**, 293.
19 K. G. Thomas, S. Barazzouk, B. I. Ipe, S. T. S. Joseph and P. V. Kamat, *J. Phys. Chem. B*, 2004, **108**, 13066.
20 (*a*) Y. Du, Y. Zhao, Y. Qu, C.-H. Chen, C.-M. Chen, C.-H. Chuang and Y. Zhu, *J. Mater. Chem. C*, 2014, **2**, 4683; (*b*) H. Nan, Z. Chen, J. Jiang, J. Li, W. Zhao, Z. Ni, X. Gu and S. Xiao, *Phys. Chem. Chem. Phys.*, 2018, **20**, 25078.
21 L. Li, X. Zheng, J. Wang, Q. Sun and Q. Xu, *ACS Sustainable Chem. Eng.*, 2013, **1**, 144.
22 A. C. Ferrari and J. Robertson, *Phys. Rev. B: Condens. Matter Mater. Phys.*, 2000, **61**, 14095.
23 Q. Zhuo, Y. Ma, J. Gao, P. Zhang, Y. Xia, Y. Tian, X. Sun, J. Zhong and X. Sun, *Inorg. Chem.*, 2013, **52**, 3141.
24 S. Laschi, I. Palchetti, G. Marrazza and M. Mascini, *J. Electroanal. Chem.*, 2006, **593**, 211.
25 (*a*) J. Chung, Y.-J. Kim and E. Yoon, *Appl. Phys. Lett.*, 2011, **98**, 123702; (*b*) J. Singh, A. Roychoudhury, M. Srivastava, V. Chaudhary, R. Prasanna, D. W. Lee, S. H. Lee and B. D. Malhotra, *J. Phys. Chem. C*, 2013, **117**, 8491; (*c*) J. Singh, P. Khanra, T. Kuila, M. Srivastava, A. K. Das, N. H. Kim, B. J. Jung, D. Y. Kim, S. H. Lee, D. W. Lee, D.-G. Kim and J. H. Lee, *Process Biochem.*, 2013, **48**, 1724; (*d*) J. Singh, A. Roychoudhury, M. Srivastava, P. R. Solanki, D. W. Lee, S. H. Lee and B. D. Malhotra, *Nanoscale*, 2014, **6**, 1195.
26 R. S. Nicholson, *Anal. Chem.*, 1965, **37**, 1351.
27 R. M. Pemberton, J. P. Hart and T. T. Mottram, *Analyst*, 2001, **126**, 1866.
28 R. J. Klingler and J. K. Kochi, *J. Am. Chem. Soc.*, 1980, **102**, 4790.
29 (*a*) T. M. Herne and M. J. Tarlov, *J. Am. Chem. Soc.*, 1997, **119**, 8916; (*b*) I. Palchetti, S. Laschi, G. Marrazza and M. Mascini, *Anal. Chem.*, 2007, **79**, 7206.
30 (*a*) T. R. Soreta, O. Y. F. Henry and C. K. Osullivan, *Biosens. Bioelectron.*, 2011, **26**, 3962; (*b*) T. Garcia-Mendiola, M. Gamero, S. Campuzano, M. Revenga-Parra, C. Alonso, M. Pedrero, F. Pariente, J. M. Pingarron and E. Lorenzo, *Anal. Chim. Acta*, 2013, **788**, 141; (*c*) D. Voccia, F. Bettazzi, E. Fratini, D. Berti and I. Palchetti, *Anal. Bioanal. Chem.*, 2016, **408**, 7271.
31 F. Bettazzi, E. Hamid-Asl, C. Esposito, C. Quintavalle, N. Formisano, S. Laschi, S. Catuogno, M. Iaboni, G. Marrazza, G. Mascini, L. Cerchia, V. De Franciscis, G. Condorelli and I. Palchetti, *Anal. Bioanal. Chem.*, 2013, **405**, 1025.
32 D. Voccia, M. Sosnowska, F. Bettazzi, G. Roscigno, E. Fratini, V. De Franciscis, G. Condorelli, R. Chitta, F. D'Souza, W. Kutner and I. Palchetti, *Biosens. Bioelectron.*, 2017, **87**, 1012.